PAPER

The use of a novel smartphone testing platform for the development of colorimetric sensor receptors for food spoilage

Tinkara Mastnak, [ID] [a] Gerhard J. Mohr [ID] [b] and Matjaž Finšgar [ID] *[a]

This work presents a novel smartphone testing platform for the validation of colorimetric sensor receptors (CSRs) in the form of layers that enables reliable and straightforward determination of their color change in a closed system using a commercially available color sensor. The food-compatible model CSR used for the method development was made of black carrot extract and ethyl cellulose. The colorimetric responses were studied in detail for NH_3, dimethylamine (DMA), and trimethylamine (TMA) by analyzing changes in the value of the total color difference (ΔE) with the increasing logarithm of the mass concentration (log γ) of the analytes. The method was partially validated for the detection limit (LOD), the limit of quantification, sensitivity, and linear γ range. The fastest reaction times were obtained for the NH_3 analyte, while the calculated LOD values were quite similar (1.48 mg L^{-1} for NH_3, 1.55 mg L^{-1} for DMA, and 1.58 mg L^{-1} for TMA). The applicability of CSRs was shown for different types of muscle food. Frozen (boneless and skinless) hake fillets were used for additional experimental work in which the color changes of the CSRs were correlated with the values of the total volatile basic nitrogen (TVB-N) and the total counts of aerobic and anaerobic microorganisms. The developed testing platform shows great promise for the development of CSRs that define the quality of a broad variety of muscle food.

1. Introduction

The predicted growth of the global population will drastically increase the pressure on the climate and the expenditure of natural resources. One of the essential actions that will enable food security for all, without further compromising delicate ecosystems, is to increase the efficiency of the entire food supply chain and reduce the amount of wasted food.[1,2]

The quantification of food waste along the food supply chain in the EU showed that 14.2 Mt of meat and 4.2 Mt of fish end up in waste annually.[3] Calculated to percentages, this means that 23% of the total meat available and 51% of the total fish available are wasted each year.

The safety systems currently used in the food processing industry rely on preventative actions in the entire life cycle of food products, including production, distribution, and post-purchase processing.[4,5] The most common solution is the simultaneous use of modified atmosphere packaging (MAP) and product refrigeration.[6] While proven to extend shelf life, these solutions do not provide information on the real state of packaged products. Their quality is usually established on the basis of safety and organoleptic properties due to a lack of objective data.[7]

Volatile amines, such as NH_3, dimethylamine (DMA), and trimethylamine (TMA) are typical representatives of one of the most frequently used parameters for monitoring muscle food quality and food safety – the total volatile basic nitrogen (TVB-N).[8] Since the TVB-N concentration increases due to microbial activity and causes an increase in the pH of the environment,[9] the development of colorimetric sensor receptors (CSRs) for muscle food is primarily based on sensing the pH inside the packaging.[10]

A sensor receptor consists of an indicator and a matrix, often a polymer. It transforms the concentration of the analyte into a quantifiable analytical signal by changing the optical properties of the indicator.[11] As the name suggests, CSRs employ visible color changes of indicators. If successfully integrated into smart food packaging, CSRs might represent a dual solution to the food waste issue by enabling prolonged shelf life and providing accurate knowledge of the points in the food supply chain where food waste is generated.

While a plethora of sensors for NH_3 and biogenic amines that might be employed for monitoring food quality have been presented, their major limitation is that some of the chemicals used for the preparation may be toxic. Even if all components are covalently linked to the sensor layer, the cleavage of covalent bonds or the breakdown of dyes during spoilage cannot be ruled out completely and contamination of food may occur. An

[a]*University of Maribor, Faculty of Chemistry and Chemical Engineering, Smetanova ulica 17, 2000 Maribor, Slovenia. E-mail: matjaz.finsgar@um.si*

[b]*JOANNEUM RESEARCH Forschungsgesellschaft mbH—Materials, Franz-Pichler-Straße 30, A-8160 Weiz, Austria*

approach that promises to provide one of the most applicable products for food applications are pH-responsive CSRs made of natural extracts and bio-based polymers. Examples from the literature include the following: alizarin and starch–cellulose paper;[12] alizarin, cellulose, and chitosan;[13] red cabbage extract mixed with chitosan and corn starch;[14] red cabbage extract and pectin;[15] mulberry extract, gelatin, and PVA;[16] curcumin and tara gum blended with PVA;[17] red radish anthocyanins in combination with gelatin and gellan gum;[18] and natural dyes extracted from the flower of *Bauhinia blakeana Dunn* immobilized in chitosan.[19]

Black or purple carrots (*Daucus carota* ssp. *sativus* var. *atrorubens* Alef.) are rich in anthocyanins and various phenolic compounds.[20] Their extracts are used as natural food colorants due to their high heat, light, and pH-stability.[21] Environmental friendliness, biodegradability, and biocompatibility make cellulose polymers sustainable substrates for the preparation of CSRs. Some examples include hydroxypropyl methylcellulose,[22] cellulose nanofibers,[23] filter paper,[24] carboxymethyl cellulose,[25] bacterial cellulose,[26] and ethyl cellulose.[27]

Straightforward and reliable determination of color changes in a closed system is of paramount importance for the development process of CSRs for food packaging applications. In preliminary studies, analysis of correlations between ΔE values and concentrations of the volatile amine analytes (NH_3, DMA, and TMA) helps us predict the applicability of CSRs. Moreover, since the composition of TVB-N is food- and spoilage-dependent, there is a need for a versatile testing platform that allows testing different food types in different environments with easily accessible and cost-effective equipment.

In order to function as laboratory-grade equipment for colorimetric detection and thus become a viable option for food monitoring applications, smartphones require accessories that enable accurate color readouts by blocking all ambient light. Furthermore, a smartphone can be paired with an external optical device (*e.g.*, a low-cost miniaturized color sensor) that enables a more accurate determination of color, generating data that can be used for decision-making.[28]

The aim of this work was to develop a novel smartphone testing platform for the validation of CSRs in the form of layers that would enable quantitative determination of their color change in a closed system using a commercially available color sensor. The CSRs used for the method development were made from black carrot extract (BCE) and ethyl cellulose, which is a hydrophobic food-compatible, chemically stable, film-forming polymer with excellent mechanical properties.[29] Due to its ability to separate gases, ethyl cellulose is partially employed for the fabrication of membranes for O_2/N_2 separations.[30] The testing platform was employed to study the colorimetric responses of CSRs to the vapors of three analytes (NH_3, DMA, and TMA). The reaction time, limit of detection (LOD), limit of quantification (LOQ), sensitivity, and linear mass concentration (γ) range were determined for each of the analytes. CSRs were further employed for the detection of the spoilage of different muscle food. The food spoilage was studied in more detail for frozen hake fillets, where colorimetric responses obtained during spoilage were correlated with the values of TVB-N, pH, and aerobic and anaerobic microbial counts.

2. Materials and methods

2.1. Chemicals and starting materials

Ammonia solution (25 wt% in H_2O), TMA solution (45 wt% in H_2O), DMA solution (40 wt% in H_2O), diethylamine ($\geq$99.5%), triethylamine ($\geq$99.5%), spermidine ($\geq$99.5%), isopentylamine (99%), ethanolamine ($\geq$98%), and ethyl cellulose were supplied by Sigma Aldrich (St. Louis, Missouri, United States of America). 1,4-Diaminobutane dihydrochloride (99%) was obtained from Alfa Aesar (Ward Hill, Massachusetts, United States of America), and ethyl acetate (ACS reagent grade) from Carlo Erba (Milan, Italy). The BCE was supplied by MAWI Chemiedistribution OHG (Limburgerhof, Germany).

Frozen South African hake (*Merluccius capensis*) fillets were purchased from a local supermarket in Maribor, Slovenia, and supplied by Seafood Connection, Urk, the Netherlands.

2.2. Preparation of the colorimetric sensor receptors

Colorimetric sensor receptors were prepared in two steps. First, 0.50 g of black carrot extract (BCE), 3.50 g of ethyl cellulose, and 70.0 mL of ethyl acetate were stirred for 24 h at 300 rpm. Second, the as prepared mixture was spread evenly onto MELINEX® ST 506 polyethylene terephthalate (PET) foil (DuPont Teijin Films, Dumfries, United Kingdom) using a double bar film applicator (BYK-Chemie GmbH, Wesel, Germany) and 380 μm PET spacers. The CSRs were left to dry under a fume hood overnight and stored in plastic containers until used in the experiments.

2.3. Experimental setup for colorimetric measurements

In order to measure the color changes of the CSRs, these were cut into circles with a 22 mm diameter and inserted under a polypropylene cap with a 15 mm center hole, suitable for a 40 mL EPA vial (Lab Logistics Group GmbH, Meckenheim, Germany). The insertion of the CSR was followed by the insertion of a 45 μm Durapore® membrane filter (PVDF membrane) of equal size and shape. Lastly, a circular hole with a diameter of 15 mm was cut into the center of the PTFE/silicone septum and the septum was inserted into the polypropylene cap (Fig. 1).

Colorimetric responses to different analytes were investigated by pipetting 10 μL of freshly prepared water solution of the respective analyte into the EPA vial and tightly screwing the previously prepared polypropylene cap (containing the CSR and the PVDF membrane). All vials were additionally sealed with parafilm and stored in a plastic container at 22 ± 1 °C.

The values of the total color difference, *i.e.*, ΔE (CIE2000),[31] were measured with a Nix QC Color Sensor (Nix Sensor Ltd., Ontario, Canada) using the default scan settings. The device was paired with a Samsung Galaxy S9 android phone (Samsung, Seoul, South Korea) *via* Bluetooth. The Nix QC Color Sensor was calibrated before each measurement according to the manufacturer's instructions. The original CSRs exposed to 10 μL of water (for an equal amount of time as the measured samples) were used as a blank. The Nix QC Color Sensor was placed on
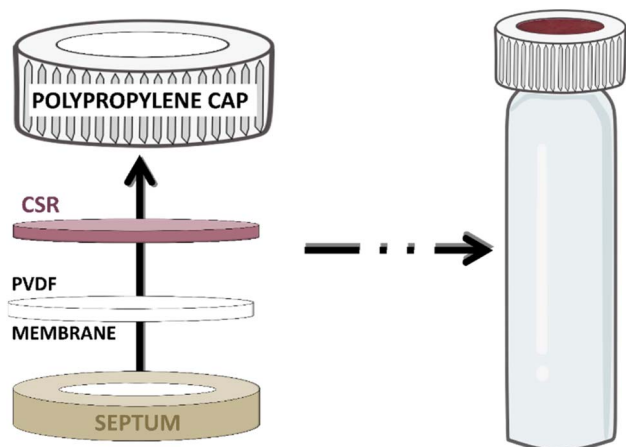
Fig. 1 A schematic presentation of the experimental setup.

the polypropylene cap flush with the surface to block out ambient light (see Fig. 2). The scanning was performed on three different places within the surface area, which permitted the proper scanning technique.

2.4. Muscle food spoilage experiments

For the preliminary muscle food spoilage experiments, 25.0 g of muscle food was weighed in a 40 mL EPA vial, which was sealed with a polypropylene cap containing the CSR. Chicken breasts and fresh trout fillets were cut into smaller pieces prior to weighing.

The frozen fish fillets used for additional spoilage experiments were defrosted overnight at 8 °C ± 1 °C and cut into thin ribbons, suitable for insertion into the 40 mL EPA vial. An equal

weight (*i.e.*, 25.0 g) of the food sample was weighed into the vial and covered with a polypropylene cap containing the CSR.

Each vial was additionally sealed with parafilm and stored in a plastic container at 22 ± 1 °C for 2, 4, 6, 8, or 10 days. Colorimetric measurements were performed as described in the previous section.

2.5. The total volatile basic nitrogen (TVB-N) determination

A fish sample (2.0 g) from the EPA vial was mixed with 100.0 mL of deionized water using a Philips Avent 4-in-1 Healthy Baby Food Maker. Then, the mixture was quantitatively transferred into a 1000 mL beaker with 900.0 mL of deionized water. Steam distillation was performed with 50.0 mL of the mixture prepared in such manner using the K12 Kjeldahl Block Digestion System (Behr Labor-Technik GmbH, Düsseldorf, Germany) until 200.0 mL of the distillate was obtained. 50.0 or 25.0 mL of the distillate was titrated with 0.02 M hydrochloric acid, and the TVB-N content was calculated according to eqn (1):

$$\text{TVB-N} = \frac{(V_1 - V_2) \cdot 14.01 \cdot c}{m} \tag{1}$$

where V_1 is the volume of the 0.02 M hydrochloric acid in mL, V_2 is the volume in mL of the 0.02 M hydrochloric acid used for the titration of the blank sample, c is the concentration of hydrochloric acid used for titration (mol L^{-1}), 14.01 is the relative atomic mass of nitrogen, and m is the weight of the fish sample (g). The analyses were performed in triplicates.

2.6. Microbiological analysis

The number of aerobic bacteria in the fish samples was determined according to ISO 4833-1:2013: the horizontal method for the enumeration of microorganisms that are able to grow and form colonies in a solid medium after aerobic incubation at 30 °C, while the number of anaerobic bacteria was determined according to the horizontal method for enumeration of anaerobic bacteria – the colony count at 30 °C by the pour plate technique. The analyses were performed by the SIST EN ISO/IEC 17025-accredited laboratory of the Faculty of Veterinary Medicine, Ljubljana, Slovenia (accreditation number LP-021).

2.7. Determination of the pH of the fish fillets

To determine the pH values of the hake fillets, 2.0 g of the fish sample was homogenized in 100.0 mL of deionized water and filtered. The pH of the filtrate was measured using a Fisherbrand™ Accumet™ Research AR25 pH Meter (Fischer Scientific, Waltham, Massachusetts, United States of America).

2.8. Materials characterization

The attenuated total reflectance-Fourier transform infrared (ATR-FTIR) spectra were recorded on a Shimadzu IRAffinity-1 ATR-FTIR device (Shimadzu Corporation, Kyoto, Japan).

The BCE samples for the ATR-FTIR measurements were exposed to water vapors or saturated vapors of NH$_3$, DMA, and TMA in the following manner: the BCE (0.10 g) was weighed into a 5.0 mL vial, and 1.0 mL of the solution was put into another
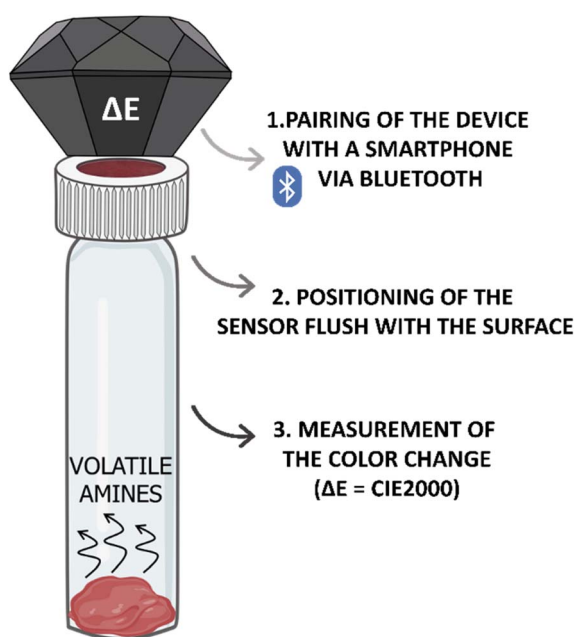

Fig. 2 A schematic illustration of the colour measurement technique.

5.0 mL vial. Both vials were carefully placed into a 100 mL borosilicate reagent glass bottle (BRAND GMBH + CO KG, Wertheim, Germany), tightly sealed, and left in the dark at room temperature for 24 hours. Then, the vial with the BCE sample was taken out of the bottle and the ATR-FTIR spectra were measured.

X-ray photoelectron spectroscopy (XPS) measurements were performed using an AXIS Supra+ device (Kratos, Manchester, UK) equipped with an Al K_α excitation source. During the XPS measurements, the charge neutralizer was turned on. The spectra were corrected using the C–C/C–H peak at 284.8 eV in the high-resolution (HR) C 1s spectra. The spectra were acquired at a 90° take-off angle. The data were acquired and processed using ESCApe 1.5 software (Kratos, Manchester, UK). HR and survey spectra were obtained at a pass energy of 20 eV and 160 eV, respectively. A Shirley background correction was performed before performing the quantitative analysis.[32]

The surface topography was determined by atomic force microscopy (AFM) and 3D-profilometry. The AFM measurements were performed in tapping mode using a MFP 3D Origin Plus instrument (Asylum/Oxford Instruments, Santa Barbara, CA, USA) with AC160TS-R3 silicon cantilevers (Asylum Research Probes, Santa Barbara, CA, USA). In order to analyze larger areas on the surface of the CSRs, a DektakXT stylus profilometer (Bruker, Karlsruhe, Germany) was used. The 3D-profiles were determined by measurements in parallel directions with a spacing of 3 μm.

3. Results and discussion

3.1 Effect of pH on the black carrot extract (BCE) in solution

The content of anthocyanins in extracts of black carrots depends on the extraction process and differs from batch to batch.[33] Since a commercial extract with an undefined composition was employed for the preparation of CSRs, we first wanted to evaluate its color changes in solutions with different pH values (Fig. 3). The observed color changes suggest the transformation of the red flavylium cation at acidic pH to a purple quinoidal anhydrobase and a blue ionized anhydrobase at pH 11.[13] At pH 13, the solution turned completely yellow, corresponding to the formation of chalcone.[34]

3.2 Colorimetric response to NH₃, DMA, TMA, and partial method validation

NH$_3$, DMA, and TMA are among the most characteristic volatile compounds associated with TVB-N.[35] For this reason, the colorimetric responses of the developed CSRs to the three analytes were quantified by analyzing changes in the value of the total color difference (ΔE) with the increasing logarithm of the mass concentration ($\log \gamma$) thereof. Prior to that, changes in the ΔE values at different γ were monitored for at least 8 days for each analyte in order to determine the times at which the colorimetric responses became constant (the reaction times).

Each analyzed data set was tested for the presence of outliers by Dixon's and Grubbs's statistical tests at 95% confidence.[36] If an outlier was detected, it was discarded and not used for the calculation. The LOD and the LOQ were determined as $3s/b_1$ and $10s/b_1$ respectively, where b_1 is the calibration curve slope and s is the standard deviation determined as the residual standard deviation (s_e) or as the standard deviation of the intercept (s_{b_0}) according to eqn (2) and (3):[37]

$$s_e = \sqrt{\frac{\sum_{j=1}^{n}(y_j - \hat{y}_j)2}{n-2}} \tag{2}$$

$$s_{b_0} = s_e \sqrt{\frac{\sum_{j=1}^{n} x_j^2}{n\left(\sum_{j=1}^{n} x_j^2 - \frac{1}{n}\left(\sum_{j=1}^{n} x_j\right)^2\right)}} \tag{3}$$

where n is the number of calibration points, y_j is the average absorbance (measured) for a particular calibration point, $\hat{y}_j$ is the absorbance of the model (which corresponds to the linear calibration curve at x_j), and x_j is the γ of a particular calibration point. The reported LOD and LOQ values are the highest calculated values calculated according to eqn (1) and (2).

The confidence limits around the linear calibration curves were determined according to eqn (4):

$$y_{\pm\text{confidence limit}} = b_0 + b_1 x_0 \pm t(\alpha, n-2) \cdot s_e \sqrt{\frac{1}{n} + \frac{(x_0 - \overline{\overline{x}})^2}{\sum_{j=1}^{n}(x_j - \overline{\overline{x}})^2}} \tag{4}$$

where $y_{\pm\text{confidence limit}}$ stands for the confidence interval value, b_0 is the intercept of the linear calibration curve, $t(\alpha, n-2)$ is the Student's t-test at confidence level α, $n-2$ represents the degrees of freedom, x_0 is the γ of the analyte, and $\overline{\overline{x}}$ is the average of γ calculated based on the γ of the calibration points used for the linear calibration curve determination.

Prior to the determination of the linear γ ranges for NH$_3$, DMA, and TMA analytes, the homogeneity of the variances was

Fig. 3 Colour changes of the BCE in solutions with increasing pH.

statistically confirmed using Bartlett's and Cochran's tests. At least six calibration points were employed for each linear γ range determination and the square of the correlation coefficient (R^2) needed to be higher than 0.99. Moreover, the quality coefficient (QC) needed to be equal to or lower than 5.00% to accept the linearity. The sensitivity was evaluated from the calibration curve slopes.[38] The results are presented in Fig. 4–6 and Table 1.

The results in Table 1 show similar LOD values for all three analytes, ranging from 1.48 mg L^{-1} for NH$_3$ to 1.55 mg L^{-1} for DMA and 1.58 mg L^{-1} for TMA. The calculated LOQ values for DMA and TMA were identical (4.47 mg L^{-1}), while the LOQ value for NH$_3$ was calculated as 3.36 mg L^{-1}. The similarity between the DMA and TMA analytes was also reflected in the determined linear γ ranges, which span from 4.45 mg L^{-1} to 89.00 mg L^{-1} for DMA and from 2.48 mg L^{-1} to 90.00 mg L^{-1} for TMA. The linear response was narrower for the NH$_3$ analyte (0.95–56.88 mg L^{-1}). The ΔE analysis showed a comparable sensitivity to NH$_3$ and DMA (10.62 log(mg L^{-1})$^{-1}$ vs. 9.87 log(mg L^{-1})$^{-1}$) but significantly lower sensitivity (i.e., 5.87 log(mg L^{-1})$^{-1}$) to the TMA analyte. It was reported previously that smaller molecules diffuse more easily across ethyl cellulose-based membranes,[39] which might explain the fastest reaction times (see the inserts in Fig. 4–6) and the lowest LOD and LOQ values for NH$_3$ (Table 1).

The bacterial decarboxylation of amino acids or the transamination of aldehydes and ketones leads to the formation of nitrogenous organic bases of low molecular weight, which are called biogenic amines (BAs).[40] BAs can be found in any type of food produced by fermentation or exposed to microbial contamination during processing or storage.[41] Therefore, various analytes can influence the pH value of the environment inside a food package. For this reason, the colorimetric responses of CSRs to an array of amine analytes were evaluated: triethylamine (Et$_3$N), spermidine (SPD), isopentylamine (IPA), diethylamine (DEA), ethanolamine (EA), and putrescine (PUT) (Fig. 7).

The ΔE values were the lowest for Et$_3$N and SPD. The exposure of the CSRs to IPA and DEA caused the color to change to violet and violet-gray, respectively. In the measurements with EA, the color changed from pink to dark grey, while the exposure of CSR to PUT caused the most significant color change, i.e., from pink to dark green, and thus the highest ΔE value. Since CSRs need to provide summative information on the total amount of amines formed during muscle food spoilage, their lack of selectivity is not problematic.[42]

3.3. Surface characterization

Fig. 8a shows the ATR-FTIR spectra of the BCE, the ethyl cellulose solution of BCE (SOL), and the CSR. The spectrum of SOL shows a peak at 1738 cm^{-1} and a peak at 1250 cm^{-1}, which correspond to the C=O and C–O in the ester group, respectively, while the peak at 1371 cm^{-1} represents C–H bending.[43] Moreover, the peak at 1045 cm^{-1} originates from a cellulose polymer[44] corresponding to C–O–C.[45] The low intensity peak at 2984 cm^{-1} for the SOL and from 2974 cm^{-1} to 2870 cm^{-1} for the CSR were attributed to the C–H stretching vibration.[46]

The anthocyanins present in black carrots mainly consist of derivatives of cyanidins, which differ in the number of sugar moieties and their degree of acylation.[47] The number of anthocyanin molecules with an increased number of sugar moieties and a high degree of acylation contribute to a intramolecular co-pigmentation effect, which is the reason for the increased heat- and light-stability and extended shelf-life of the BCE.[33] The anthocyanins in BCE in Fig. 8b are characterized by the peak at 1035 cm^{-1}, which corresponds to the C–H
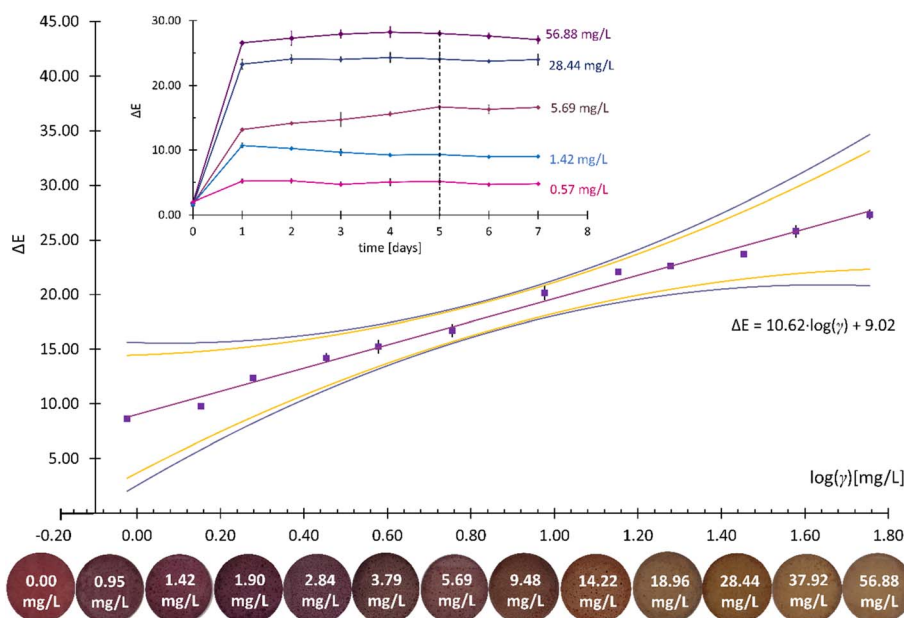

Fig. 4 The calibration curve with 90% and 95% confidence intervals for the NH$_3$ analyte with the corresponding color changes and changes in the value of ΔE at different γ with increasing time (insert). Error bars represent standard deviations.
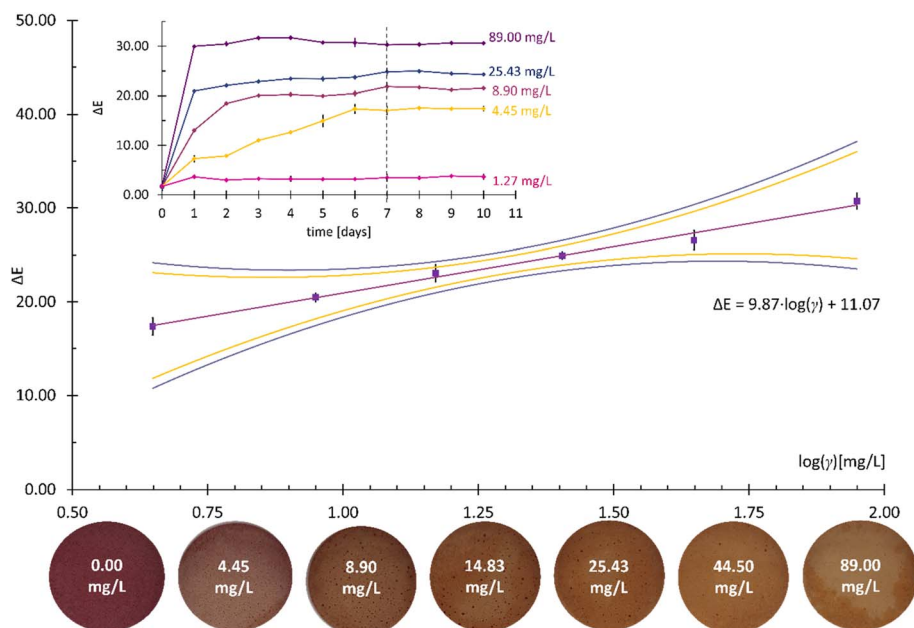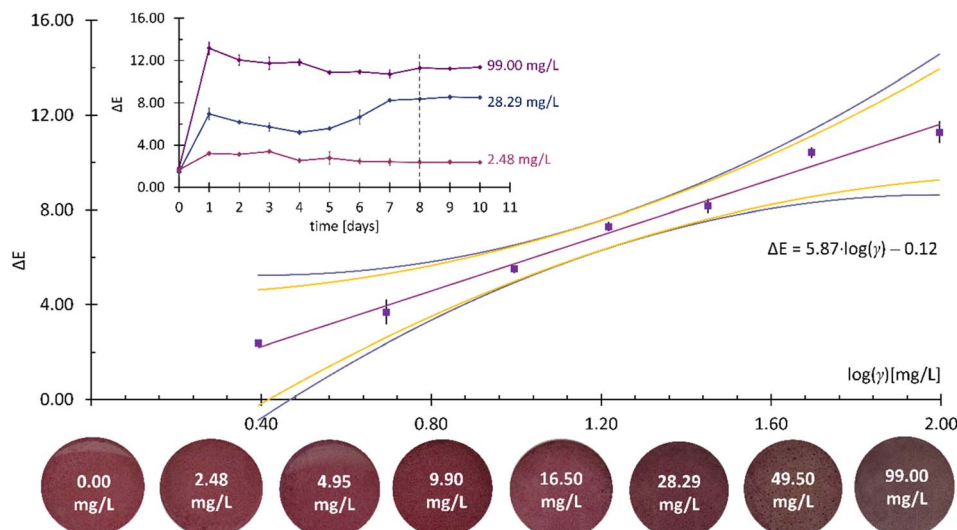
Fig. 5 The calibration curve with 90% and 95% confidence intervals for the DMA analyte with the corresponding color changes and changes in the value of ΔE at different γ with increasing time (insert). The error bars represent standard deviations.

Fig. 6 The calibration curve with 90% and 95% confidence intervals for the TMA analyte with corresponding color changes and changes in the value of ΔE at different γ with increasing time (insert). The error bars represent standard deviations.

Table 1 Summary of the statistical tests and analytical characteristics of the CSRs for the detection of NH_3, DMA, and TMA

Analyte	NH_3	DMA	TMA
Reaction time (days)	5	7	8
Grubbs's and Dixon's outlier tests	Passed	Passed	Passed
LOD (mg L^{-1})	1.48	1.55	1.58
LOQ (mg L^{-1})	3.36	4.47	4.47
Bartlett's and Cochran's tests	Passed	Passed	Passed
Linear γ range (mg L^{-1})	0.95–56.88	4.45–89.00	2.48–90.00
R^2	0.99	0.99	0.99
Sensitivity (log(mg L^{-1})$^{-1}$)	10.62	9.87	5.87

deformation of the aromatic ring,[48] and the C=O stretching at 1632 cm^{-1} for the BCE exposed to water vapors (BCE–H_2O), and at 1565 cm^{-1} for the BCE exposed to the saturated vapors of different amine analytes (BCE–NH_3, BCE–DMA, and BCE–TMA).[49] The peaks at around 1260 cm^{-1} were attributed to the C–C vibrations,[50] while the peaks at around 1400 cm^{-1} correspond to the stretching vibrations of the aromatic ring.[48] The broad band from 3000 cm^{-1} to 3700 cm^{-1} indicates the presence of O–H vibrations and the formation of hydrogen bonds[51] and is much more pronounced in the spectra of the BCE samples exposed to the (water-based) solutions.
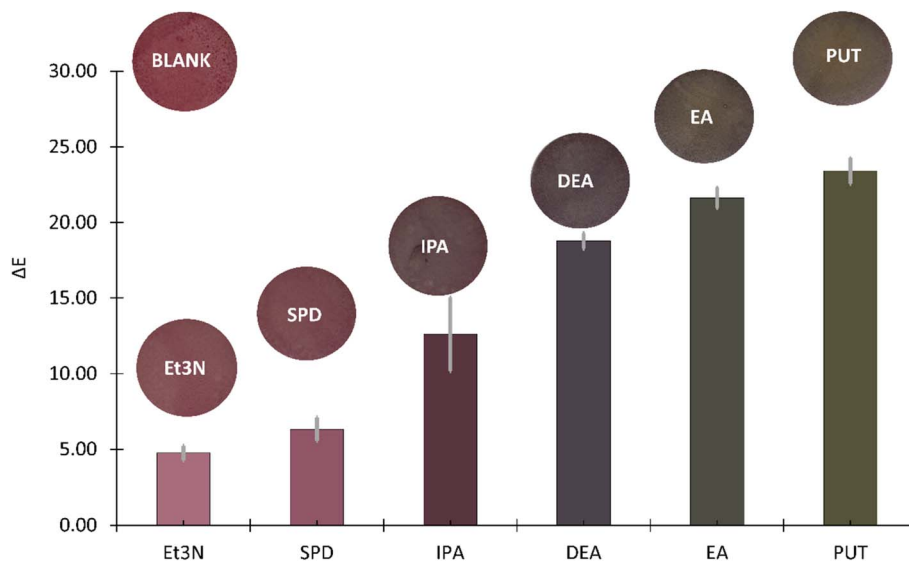
Fig. 7 The colorimetric responses of the CSRs after 24 h to different amines. The error bars represent standard deviations.

Since there are no significant variations in the intensity or position of the signals in the ATR-FTIR spectra after the exposure of the BCE to the amine analytes, this indicates that no chemical reaction occurred and that the exposure to the saturated vapors of amines had no influence on the molecular structure of the BCE.

To further confirm the surface species suggested by the ATR-FTIR measurements, an XPS surface analysis was performed. Fig. 9 shows the HR spectra, survey spectra, and the quantitative results for the C-containing species for the CSR that was exposed to water vapors (BLANK), the CSR before exposure to water vapors (DRY), the CSR that was exposed to saturated vapors of ammonia (NH_3), and the CSR exposed to daylight for 10 months (UV). For all four samples, the C 1s signal was detected originating from organic compounds as suggested by the ATR-FTIR analysis explained above. The C 1s spectra were deconvoluted into four peaks at different binding energies: C–

C/C–H at 284.8 eV, C–O at 286.3 eV, C=O at 287.7 eV, and COO/COOH at 289.1 eV (Fig. 9a–d). Based on the deconvoluted peaks, the surface atomic concentration of these species was determined (Fig. 9e). The slight differences in their contents were most probably caused by changes in the composition of the pH-dependent anthocyanins in the BCE.[52]

Since all four samples contain oxidized organic species on the surface (which was also confirmed by ATR-FTIR measurements), the O 1s signal corresponding to the C–O, C=O, and COO/COOH species on the surface was obtained (Fig. 9f). In addition, the N signal with low intensity was also detected on the surface of NH_3 samples, probably due to the residue of the NH_3 analyte (Fig. 9g). Besides C- and O-containing species, Si was also detected (the Si 2p and Si 2s peaks in Fig. 9h), possibly originating from the manufacturing process of the PET foil or from the residues of the carbon tape used for the attachment of samples.
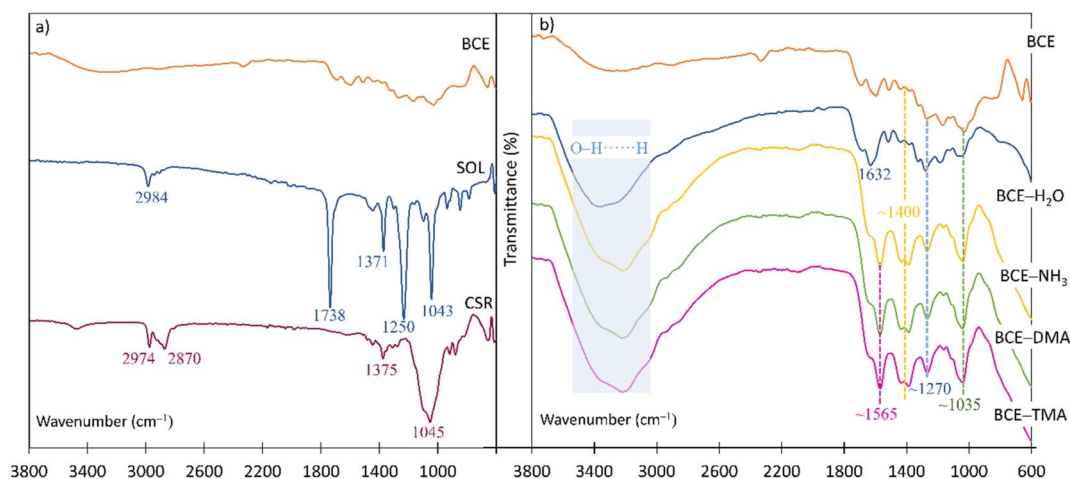

Fig. 8 (a) The ATR-FTIR spectra of the BCE, the SOL, and the CSR; (b) the ATR-FTIR spectra of the BCE, the BCE–H_2O, and the BCE exposed to saturated vapors of NH_3, DMA, and TMA.
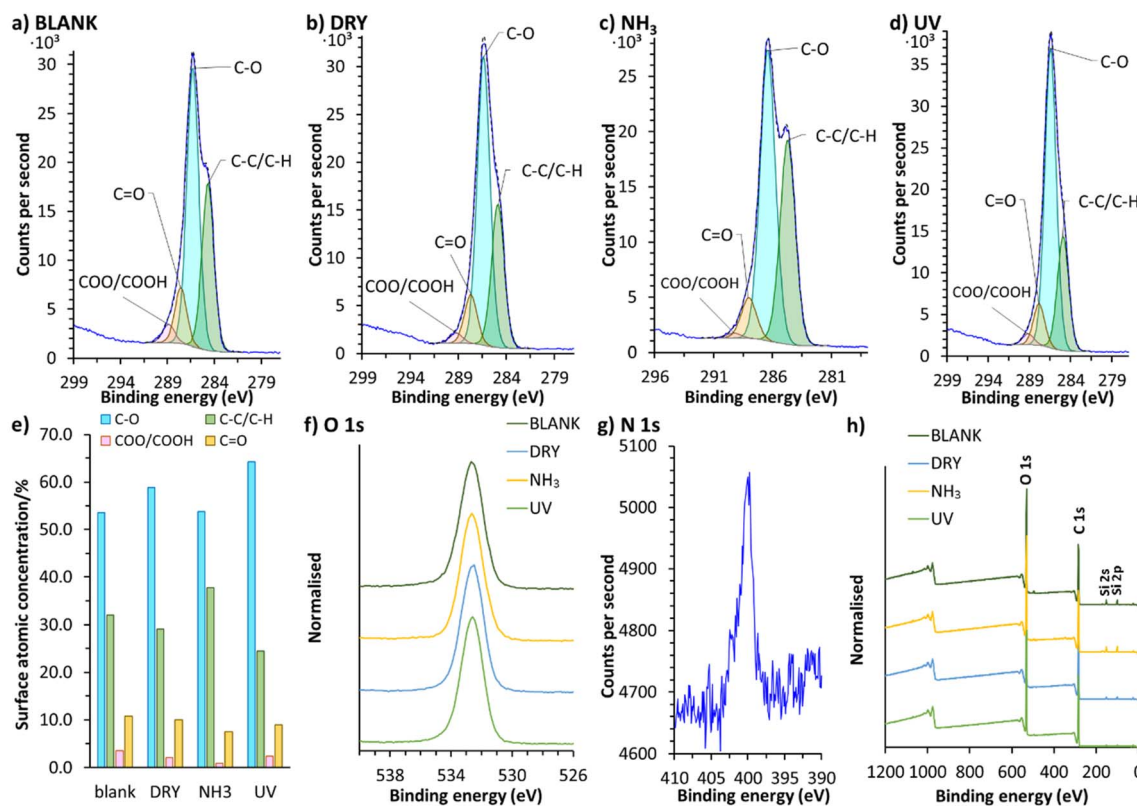
Fig. 9 Deconvoluted HR C 1s spectra of the (a) BLANK, (b) DRY, (c) NH$_3$, and (d) UV samples, and (e) the surface atomic concentration of the C-containing species, (f) the HR O 1s spectra, (g) the HR N 1s spectrum of the NH$_3$ sample, and (h) the survey spectra.
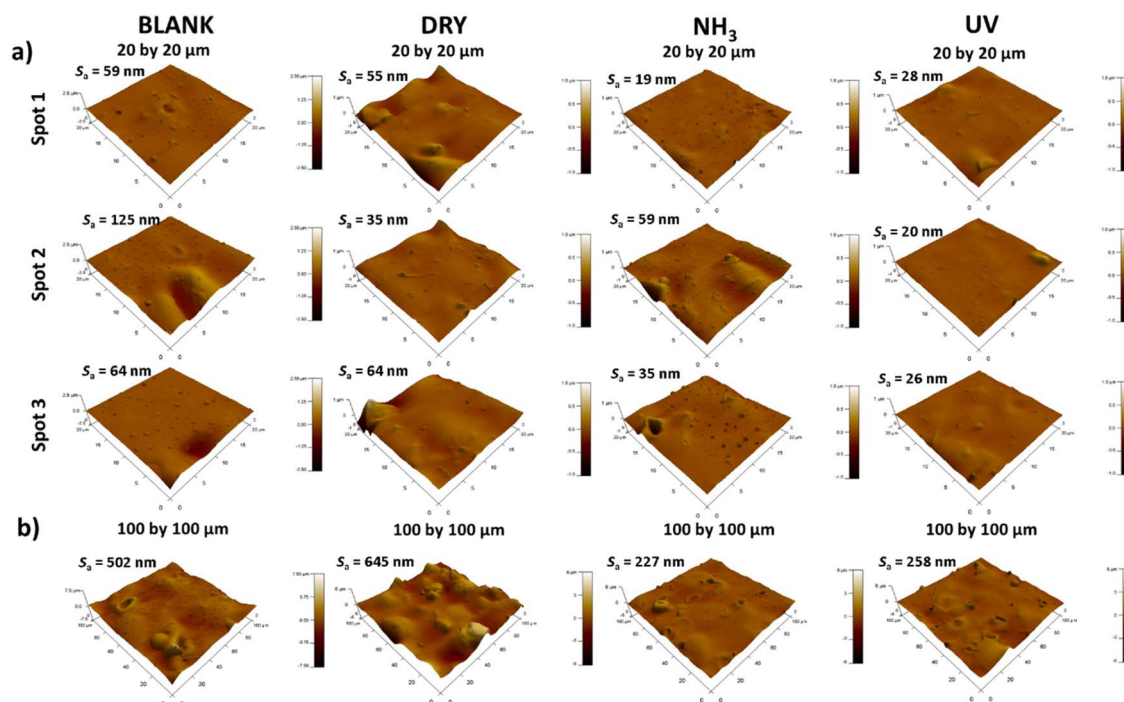

Fig. 10 AFM 3D images of the BLANK, DRY, NH$_3$, and UV samples measured on (a) 20 by 20 μm (three spots) and (b) 100 by 100 μm (one spot) areas on the surface.

To conclude, the XPS surface analysis showed no significant differences between the DRY and UV samples, which suggests that the developed CSRs are UV-stable and have a shelf life of at least 10 months.

The topography of the samples studied by means of XPS was additionally evaluated by AFM (Fig. 10) and 3D-profilometry (Fig. 11). The surface profiles in Fig. 10 and 11 provide information on the mean surface roughness (S_a), which is based on the general surface roughness. The higher the S_a value, the rougher the surface is. The AFM measurements were performed on three different 20 by 20 μm spots (Fig. 10a) and on one spot with an area of 100 by 100 μm (Fig. 10b), while the surface topography using 3D-profilometry was obtained on a significantly larger scale, *i.e.*, on an area 2 by 2 mm. The differences in the surface features of the samples are not significant. However, some variations exist since the CSRs were prepared manually. However, these differences do not affect the performance characteristics of the presented CSRs.

3.4. The application of the CSRs for the detection of muscle food spoilage

The applicability of the developed CSRs was first tested in preliminary experiments with different types of muscle food (Fig. 12). Minced beef, minced poultry, chicken breast, and fresh trout samples were spoiled at 22 ± 1 °C for 5 and 10 days. The results after 5 days showed very subtle color changes in the CSRs in contact with the minced beef samples, while the most significant color changes occurred in the CSRs that were in contact with the fish samples. After 10 days, all color differences became much more pronounced, which was reflected in the changes in the corresponding ΔE values. The increase in the ΔE values ranged from 75% for the minced beef and up to 270% for the trout samples. The results are not surprising, since fish is known to have a particularly heavy microbial load.[53]

While the process of muscle food spoilage is diverse and depends on the food type, microorganisms present, and environment (temperature, the presence of air), common chemicals (BAs; see above) are produced in high levels as a consequence of intensive microbial activity.[38] However, there is a lack of consistency in the data as to the presence of BAs due to their challenging identification and quantification. One of the underlying reasons is that their concentration depends on the intrinsic properties of foodstuffs, such as moisture content, fat, protein, and pH value. These provide a rich milieu for the development of microorganisms and biochemical reactions, making the food perishable during processing and storage.[40] Since the size of samples used for the spoilage experiments was rather small, it was particularly important that the muscle food samples had as much constant composition as possible. For this reason, frozen (boneless and skinless) hake fillets were used for additional experimental work.

The color changes detected during the more detailed spoilage experiments are presented in Fig. 13.

A comparison between the results obtained in preliminary experiments with fresh trout (Fig. 12) shows that the color changes of the CSRs obtained on day 10 in Fig. 13 are much less
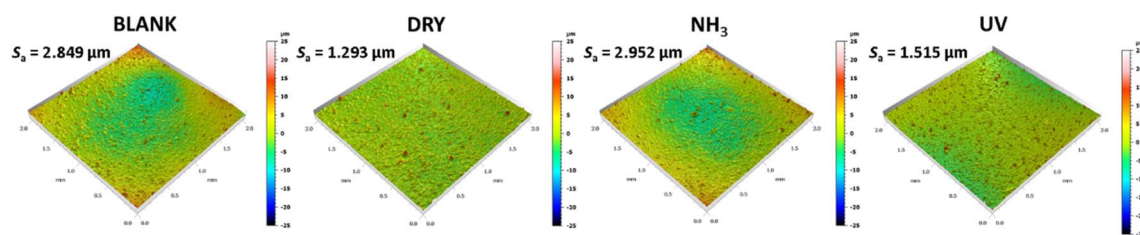

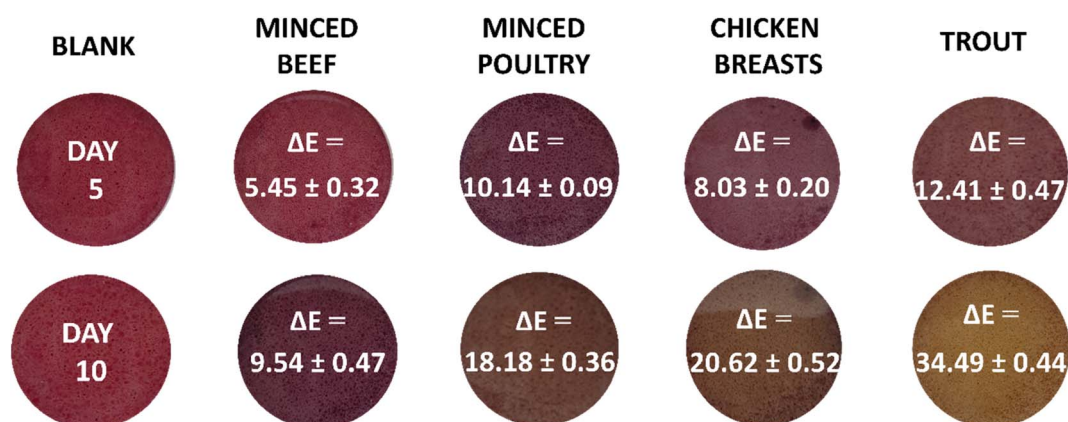Fig. 11 3D-profiles measured on 2 by 2 mm spot sizes for BLANK, DRY, NH₃, and UV samples.

Fig. 12 The color changes and corresponding ΔE values of the CSRs during spoilage experiments with different types of muscle food. The ΔE values are presented with standard deviations.

pronounced. The reason for this lies in the fact that there are considerable variations in the formation of volatile amines between species and types of products.[54] However, the aim of this work was to establish a testing platform for the colorimetric evaluation of muscle food spoilage in a closed system, not a study of muscle food spoilage *per se*. As mentioned above, the choice of the fish product was based on the desire to ensure a constant composition of the food samples during the method development process.

3.3.1. The determination of the total volatile basic nitrogen (TVB-N) in fish samples. The TVB-N determined in the flesh of fish is a potential freshness indicator due to the presence of volatile amines, such as TMA, DMA, and NH_3, which are responsible for the characteristic 'fishy' odor typical of spoiled fish.[55] The degradation of proteins during storage results in the accumulation of TVB-N, causing an increase in the pH value, which provides better growth conditions for such microorganisms.[56] Therefore, there is generally a strong positive correlation between an increasing pH value and the concentration of TVB-N. Such a trend can also be observed in Fig. 14, which shows the TVB-N and pH values of spoiled hake samples during the 10 day period.

The results show a general increase in the content of TVB-N throughout the duration of the spoilage experiments. The value of TVB-N from day 0 to day 2 increased only for 0.11 mg/100 g of the fish sample (from 12.99 mg/100 g to 13.10 mg/100 g). A similar trend can be observed when comparing the results from day 6 (16.08 mg/100 g) and day 8 (16.25 mg/100 g). On the last (10th) day of the experiment, the fish samples had an incredibly foul odor and were visibly spoiled, but the amount of TVB-N reached only 17.24 mg/100 g, which is well below the legal maximum allowed by the European Commission (*i.e.*, 35 mg/100 g of the sample).[57] This shows that the TVB-N values need to be considered with caution and viewed in the context of other spoilage parameters. Moreover, the relevant TVB-N thresholds for food safety need to be established for each muscle food type and for each storage condition.
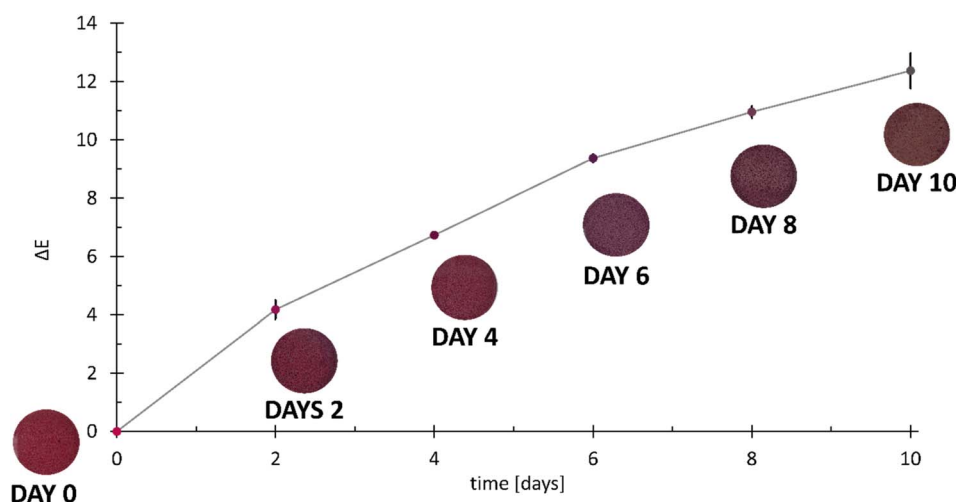

Fig. 13 Spoilage experiments conducted with frozen hake fillets (*Merluccius capensis*) showing photos of the CSRs and the corresponding ΔE values. The error bars represent standard deviations.
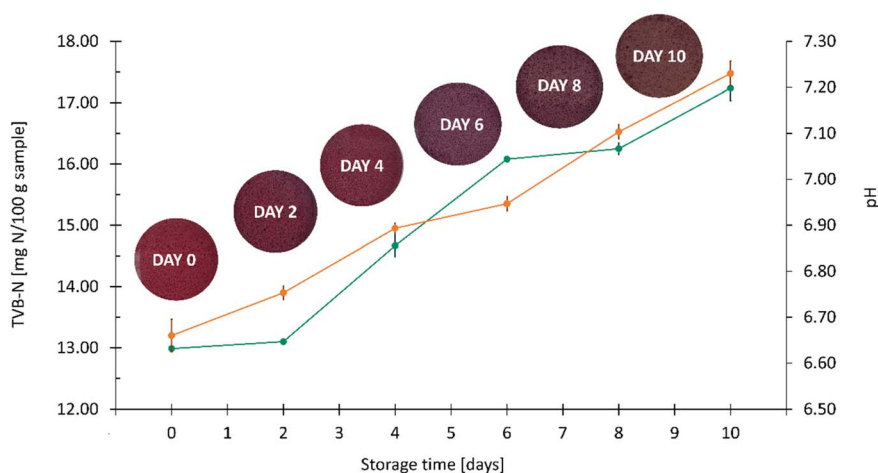

Fig. 14 The TVB–N (turquoise) and pH values (orange) of spoiled fish samples during the 10 day period, with corresponding color changes of the CSRs. The error bars represent standard deviations.
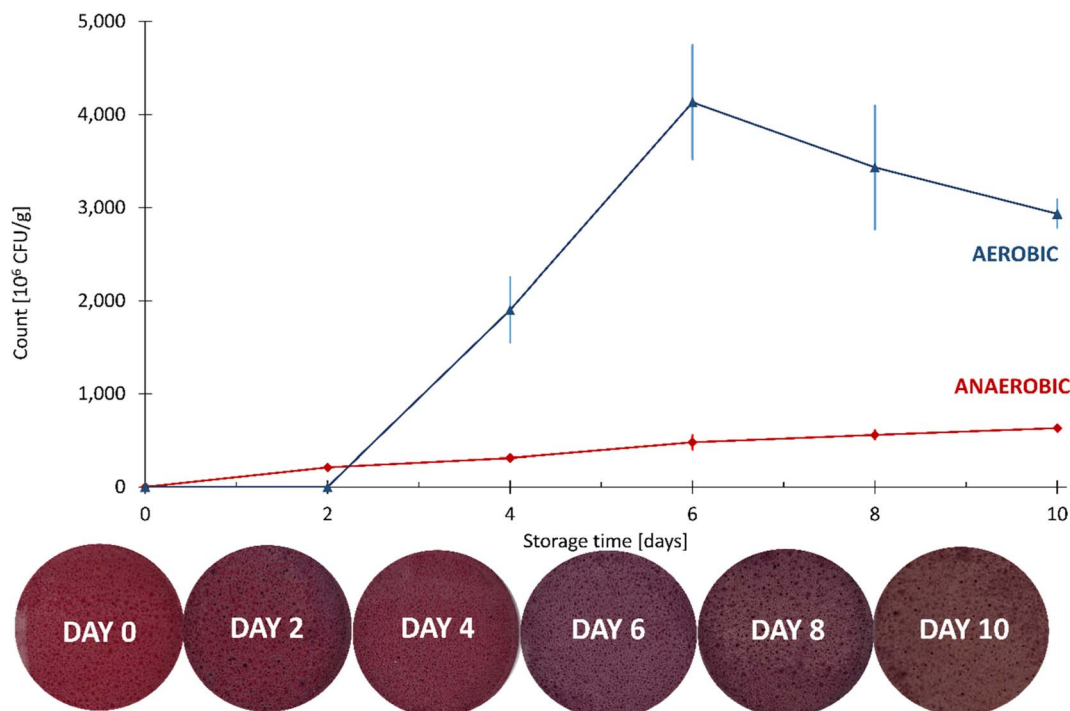
Fig. 15 The aerobic and anaerobic counts of the fish samples during the 10 day spoilage experiment, with the corresponding color changes of the CSRs. The error bars represent standard deviations.

3.3.2. Microbiological analysis of fish. It has been well established that the TVB-N content in muscle food increases with storage time and that its accumulation pattern correlates with the microbial count.[58] Several microorganisms produce NH_3 and methylamines and thus contribute to the TVB-N levels. The dynamics and growth of microbial species depend on the availability of oxygen and the preferred substrate, moisture, and pH of the environment.[59]
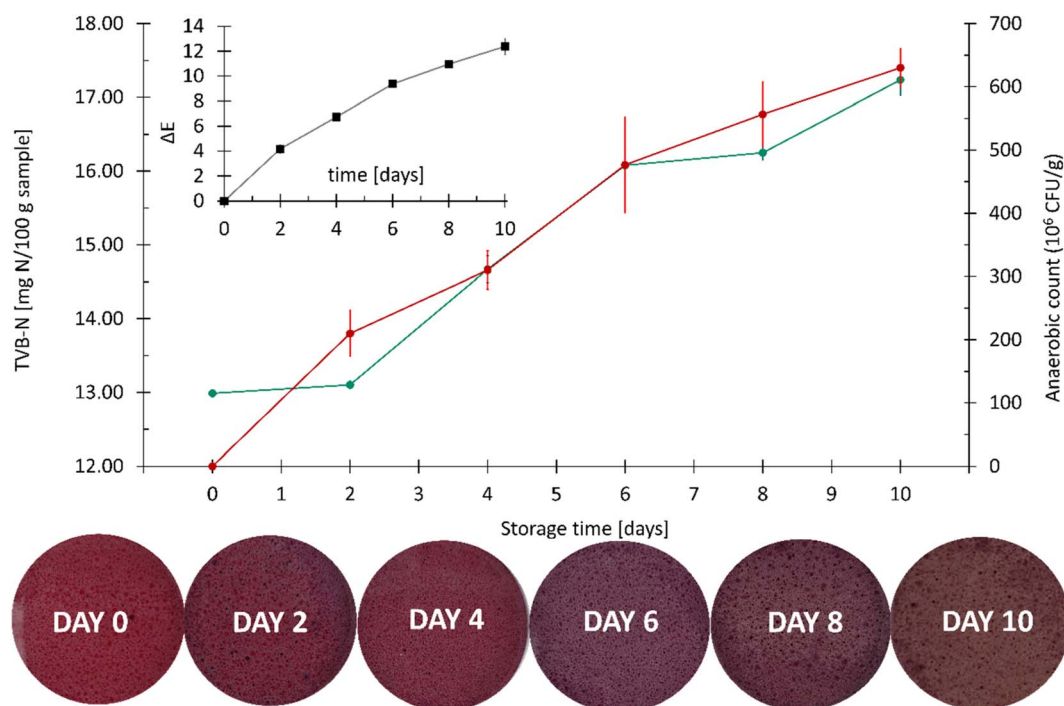

Fig. 16 The correlation between TVB-N (turquoise) and the anaerobic bacterial count (red) with representative colors of the CSRs. The insert shows the changes in the values of ΔE. The error bars represent standard deviations.

Since the tightly sealed vials contained a limited amount of oxygen, the fish samples were analyzed for the total number of aerobic bacteria and the total number of anaerobic bacteria (Fig. 15).

Compared to the anaerobic count, the aerobic count was greater by an order of magnitude on each day of the analysis. An insignificant change in the number of aerobic microorganisms at day 2 was followed by a large increase on the following two measuring dates, reaching approximately 4×10^9 CFU g^{-1} on day 6. After that, a fall in the count in the aerobic microorganisms was observed, most probably due to the depletion of oxygen required for their growth. On the other hand, the number of anaerobic microorganisms increased steadily throughout the experiment, reaching approximately 4×10^8 CFU g^{-1} on day 10.

The total numbers of microorganisms in fish vary enormously. Data published by the Food and Agriculture Organization (FAO) show that the total number of microorganisms in the gills and intestines of fresh fish spans from 10^2 CFU g^{-1} up to 10^9 CFU g^{-1}.[60] The level of microbial spoilage therefore depends on the initial microbial composition of fish, the degree of processing and preservation, together with chemical composition and storage temperature.[53]

The functioning of spoilage microorganisms is often associated with a food product defect, such as the presence of TVB-N (Fig. 16).

Fig. 16 shows a strongly positive correlation between the values of TVB-N and the anaerobic count of microorganisms. Many different species of microorganisms from very different sources may cause food spoilage, even in a selective environment based on a defined food formulation. The mechanism of BA production through the decarboxylation of various amino acids has been reported for several classes of microorganisms.[61] However, one needs to keep in mind that not all microorganisms are able to decarboxylate free amino acids, so low concentrations of amines do not necessarily signal good microbiological quality,[40] which was also confirmed by our results.

4. Conclusion

Food-compatible CSRs enable the flexible, robust, non-destructive sensing, easy miniaturization, and fabrication of low-cost, and sustainable systems. This work presents an affordable and versatile testing platform for the validation thereof in a closed system, using a commercial color sensor. The method enables the systematic evaluation of color changes in terms of ΔE values and their correlation with potential food spoilage indicators (TVB-N and microbial profile).

The CSRs used for the development of the method described herein were made from black carrot extract and ethyl cellulose. Their colorimetric responses to increasing logarithms of mass concentrations ($\log \gamma$) of the vapors of three analytes (NH_3, DMA, and TMA) were studied. The method was partially validated for the limit of detection (LOD), the limit of quantification (LOQ), sensitivity, and linear γ range. The LOD values ranged from 1.48 mg L^{-1} for NH_3, to 1.55 mg L^{-1} for DMA and 1.58 mg L^{-1} for TMA. The calculated LOQ values for DMA and TMA were identical (4.47 mg L^{-1}), while the LOQ value for NH_3 was calculated to be 3.36 mg L^{-1}. Similarity between the DMA and the TMA analytes was also reflected in the determined linear γ ranges. The ΔE analysis showed comparable sensitivity for NH_3 and DMA but significantly lower sensitivity for the TMA analyte. Overall, the fastest reaction times and the best analytical characteristics were obtained for the NH_3.

The presented novel smartphone testing platform shows great promise and might pave the way to the successful development of colorimetric devices that define the quality of a broad variety of muscle food. This could result in solutions for smart food packaging that enable monitoring of food quality and food safety, while expanding nominal shelf life and reducing food waste.

Author contributions

Tinkara Mastnak: conceptualization, methodology, validation, formal analysis, investigation, writing – original draft, visualization. Gerhard J. Mohr: conceptualization, resources, methodology, investigation, writing – review & editing. Matjaž Finšgar: writing – original draft, validation, formal analysis, writing – review & editing, resources, funding acquisition.

Conflicts of interest

The authors declare that they have no known competing financial interests or personal relationships that could appear to influence the work reported in this paper.

Acknowledgements

References

1 L. H. Nguyen, S. Naficy, R. McConchie, F. Dehghani and R. Chandrawati, *J. Mater. Chem. C*, 2019, **7**, 1919–1926.

2 M. Weston, A.-H. Pham, J. Tubman, Y. Gao, A. D. Tjandra and R. Chandrawati, *Mater. Adv.*, 2022, **3**, 4088–4102.

3 C. Caldeira, V. De Laurentiis, S. Corrado, F. van Holsteijn and S. Sala, *Resour., Conserv. Recycl.*, 2019, **149**, 479–488.

4 G.-J. E. Nychas, P. N. Skandamis, C. C. Tassou and K. P. Koutsoumanis, *Meat Sci.*, 2008, **78**, 77–89.

5 F. Arshad, N. F. Mohd-Naim, R. Chandrawati, D. Cozzolino and M. U. Ahmed, *RSC Adv.*, 2022, **12**, 26160–26175.

6 L. E. Jeremiah, *Food Res. Int.*, 2001, **34**, 749–772.

7 A. Dehaut, C. Himber, V. Mulak, T. Grard, F. Krzewinski, B. Le Fur and G. Duflos, *J. Agric. Food Chem.*, 2014, **62**, 8014–8022.

8 H.-N. Chun, J.-H. Cho and H.-S. Shin, *Food Sci. Biotechnol.*, 2014, **23**, 1411–1416.

9 M. Moradi, H. Tajik, H. Almasi, M. Forough and P. Ezati, *Carbohydr. Polym.*, 2019, **222**, 115030.

10 N. Oladzadabbasabadi, A. Mohammadi Nafchi, M. Ghasemlou, F. Ariffin, Z. Singh and A. A. Al-Hassan, *Food Packag. Shelf Life*, 2022, **33**, 100872.

11 J. Dakin and B. Culshaw, *Chemical Sensing Using Indicator Dyes*, 1997, pp. 53–107.

12 P. Ezati, H. Tajik, M. Moradi and R. Molaei, *Int. J. Biol. Macromol.*, 2019, **132**, 157–165.

13 P. Ezati, H. Tajik and M. Moradi, *Sens. Actuators, B*, 2019, **285**, 519–528.

14 M. C. Silva-Pereira, J. A. Teixeira, V. A. Pereira-Júnior and R. Stefani, *LWT–Food Sci. Technol.*, 2015, **61**, 258–262.

15 I. Dudnyk, E.-R. Janeček, J. Vaucher-Joset and F. Stellacci, *Sens. Actuators, B*, 2018, **259**, 1108–1112.

16 P. Zeng, X. Chen, Y.-R. Qin, Y.-H. Zhang, X.-P. Wang, J.-Y. Wang, Z.-X. Ning, Q.-J. Ruan and Y.-S. Zhang, *Food Res. Int.*, 2019, **126**, 108604.

17 Q. Ma, L. Du and L. Wang, *Sens. Actuators, B*, 2017, **244**, 759–766.

18 X. Zhai, Z. Li, J. Zhang, J. Shi, X. Zou, X. Huang, D. Zhang, Y. Sun, Z. Yang, M. Holmes, Y. Gong and M. Povey, *J. Agric. Food Chem.*, 2018, **66**, 12836–12846.

19 X. Zhang, S. Lu and X. Chen, *Sens. Actuators, B*, 2014, **198**, 268–273.

20 A. Smeriglio, M. Denaro, D. Barreca, V. D'Angelo, M. P. Germanò and D. Trombetta, *Fitoterapia*, 2018, **124**, 49–57.

21 E. C. Montilla, M. R. Arzaba, S. Hillebrand and P. Winterhalter, *J. Agric. Food Chem.*, 2011, **59**, 3385–3390.

22 J. Huang, J. Liu, M. Chen, Q. Yao and Y. Hu, *Int. J. Biol. Macromol.*, 2021, **184**, 666–677.

23 S. Roy and J.-W. Rhim, *Food Hydrocolloids*, 2021, **114**, 106566.

24 S. U. Haq, M. Aghajamali and H. Hassanzadeh, *RSC Adv.*, 2021, **11**, 24387–24397.

25 M. Kurek, L. Hlupić, M. Ščetar, T. Bosiljkov and K. Galić, *J. Food Sci.*, 2019, **84**, 2490–2498.

26 S. Mohammadalinejhad, H. Almasi and M. Moradi, *Food Control*, 2020, **113**, 107169.

27 J. Fan, S. Zhang, F. Li, Y. Yang and M. Du, *Cellulose*, 2020, **27**, 9157–9179.

28 S. Nag, A. Mondal, H. Hirani and P. Banerjee, *Mater. Adv.*, 2022, **3**, 4649–4658.

29 J. Xu, H. Jia, N. Yang, Q. Wang, G. Yang, M. Zhang, S. Xu, Y. Zang, L. Ma, P. Jiang, H. Zhou and H. Wang, *Polymers*, 2019, **11**, 1900.

30 M. Minelli and G. C. Sarti, *J. Membr. Sci.*, 2015, **473**, 137–145.

31 G. Sharma, W. Wu and E. N. Dalal, *Color Res. Appl.*, 2005, **30**, 21–30.

32 D. A. Shirley, *Phys. Rev. B*, 1972, **5**, 4709–4714.

33 S. Kamiloglu, J. Van Camp and E. Capanoglu, *Phytochem. Rev.*, 2018, **17**, 379–395.

34 C. M. P. Yoshida, V. B. V. Maciel, M. E. D. Mendonça and T. T. Franco, *LWT–Food Sci. Technol.*, 2014, **55**, 83–89.

35 M. Moosavi-Nasab, S. Khoshnoudi-Nia, Z. Azimifar and S. Kamyab, *Sci. Rep.*, 2021, **11**, 5094.

36 B. Slutsky, *J. Chem. Inf. Comput. Sci.*, 1998, **38**, 1254.

37 J. N. Miller, *Analyst*, 1991, **116**, 3–14.

38 T. Mastnak, A. Lobnik, G. J. Mohr and M. Finšgar, *Sensors*, 2018, **18**, 4361.

39 X.-G. Li, I. Kresse, Z.-K. Xu and J. Springer, *Polymer*, 2001, **42**, 6801–6810.

40 M. Papageorgiou, D. Lambropoulou, C. Morrison, E. Kłodzińska, J. Namieśnik and J. Płotka-Wasylka, *TrAC, Trends Anal. Chem.*, 2018, **98**, 128–142.

41 F. Aflaki, V. Ghoulipour, N. Saemian and M. Salahinejad, *Anal. Methods*, 2014, **6**, 1482–1487.

42 C. Schaude, C. Meindl, E. Fröhlich, J. Attard and G. J. Mohr, *Talanta*, 2017, **170**, 481–487.

43 A. El Nemr, S. Ragab, A. El Sikaily and A. Khaled, *Carbohydr. Polym.*, 2015, **130**, 41–48.

44 J. Song, N. L. Birbach and J. P. Hinestroza, *Cellulose*, 2012, **19**, 411–424.

45 Y. Kim, D. Jeong, K. H. Park, J.-H. Yu and S. Jung, *Polymers*, 2018, **10**, 1042.

46 R. Md Salim, J. Asik and M. S. Sarjadi, *Wood Sci. Technol.*, 2021, **55**, 295–313.

47 E. Agcam, A. Akyıldız and V. M. Balasubramaniam, *Food Chem.*, 2017, **237**, 461–470.

48 X. Zhang, Y. Liu, H. Yong, Y. Qin, J. Liu and J. Liu, *Food Hydrocolloids*, 2019, **94**, 80–92.

49 J. Huang, Z. Hu, G. Li, L. Hu, J. Chen and Y. Hu, *Trends Food Sci. Technol.*, 2022, **124**, 259–277.

50 S. Pourjavaher, H. Almasi, S. Meshkini, S. Pirsa and E. Parandi, *Carbohydr. Polym.*, 2017, **156**, 193–201.

51 T. Maver, T. Mastnak, M. Mihelič, U. Maver and M. Finšgar, *Materials*, 2021, **14**, 1464.

52 C. C. Gras, H. Bogner, R. Carle and R. M. Schweiggert, *Food Res. Int.*, 2016, **85**, 291–300.

53 M. Sivertsvik, in *Novel Food Packaging Techniques*, ed. R. Ahvenainen, Woodhead Publishing, 2003, pp. 384–400, DOI: **10.1533/9781855737020.3.384**.

54 R. Mendes, H. Silva, P. Oliveira, L. Oliveira and B. Teixeira, *Foods*, 2021, **10**, 848.

55 N. Wells, D. Yusufu and A. Mills, *Talanta*, 2019, **194**, 830–836.

56 J. Miao, W. Peng, G. Liu, Y. Chen, F. Chen and Y. Cao, *Food Control*, 2015, **56**, 53–56.

57 *Commission Regulation (EC) No. 1022/2008 of 17 October 2008 amending Regulation (EC) No. 2074/2005 as regards the total volatile basic nitrogen (TVB-N) limits*, 2008.

58 A. E.-D. A. Bekhit, S. G. Giteru, B. W. B. Holman and D. L. Hopkins, *Compr. Rev. Food Sci. Food Saf.*, 2021, **20**, 3620–3666.

59 A. E.-D. A. Bekhit, B. W. B. Holman, S. G. Giteru and D. L. Hopkins, *Trends Food Sci. Technol.*, 2021, **109**, 280–302.

60 *Code of conduct for responsible fisheries*, Food and Agriculture Organization of the United Nations, Rome, 1995.

61 J. W. Sanders, S. J. C. M. Oomes, J. M. Membré, A. Wegkamp and M. Wels, *Food Microbiol.*, 2015, **45**, 34–44.